Beyond the standard model of solubilization: Non-ionic surfactants induce collapse of lipid vesicles into rippled bilamellar nanodiscs
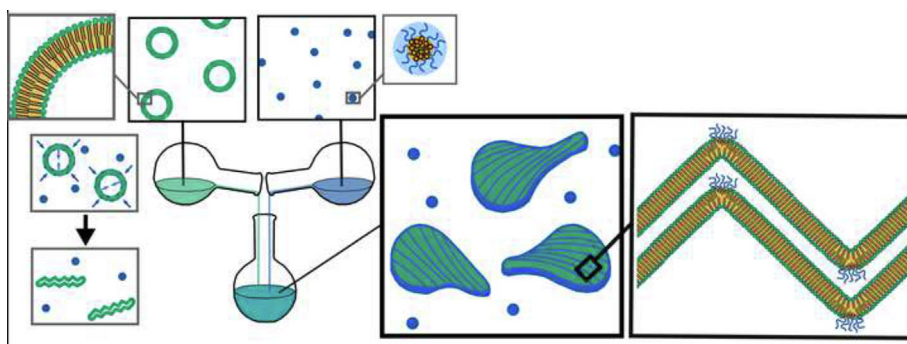
Victoria Ariel Bjørnestad [a], Fernando Soto-Bustamante [b], Giancarlo Tria [b], Marco Laurati [b], Reidar Lund [a,*]

[a] Department of Chemistry, University of Oslo, Sem Sælandsvei 26, 0371 Oslo, Norway
[b] Department of Chemistry and CSGI, University of Florence, Sesto Fiorentino, Italy

GRAPHICAL ABSTRACT

ARTICLE INFO

ABSTRACT

Hypothesis: Although solubilization of lipid membranes has been studied extensively, questions remain regarding the structural pathways and metastable structures involved. This study investigated whether the non-ionic detergent Triton X-100 follows the classical solubilization pathway or if intermediate nanostructures are formed.

Experiments: Small angle X-ray and neutron scattering (SAXS/SANS) was used in combination with transmission electron cryo-microscopy and cryo-tomography to deduce the structure of mixtures of 1,2-dipalmitoyl-*sn*-glycero-3-phosphocholine (DPPC) vesicles and Triton X-100. Time-resolved SAXS and dynamic light scattering were used to investigate the kinetics of the process.

Findings: Upon addition of moderate detergent amounts at low temperatures, the lipid vesicles implode into ordered rippled bilamellar disc structures. The bilayers arrange in a ripple phase to accommodate packing constraints caused by inserted TX-100 molecules. The collapse is suggested to occur through a combination of water structure destabilization by detergents flipping across the membrane and osmotic pressure causing interbilayer attraction internally. The subsequently induced ripples then stabilize the aggregates and prevent solubilization, supported by the observation that negatively charged vesicles undergo a different pathway upon TX-100 addition, forming large bicelles. The findings demonstrate

the richness in assembly pathways of simple lipids and detergents and stimulate considerations for the use of certain detergents in membrane solubilization.

1. Introduction

The Triton X-series of surfactants is one of the most utilized detergents for biotechnological applications. They all share a common tail group consisting of hydrophobic p-tertoctylphenyl and are separated by differences in the length of the hydrophilic oligo-ethylene oxide (EO) headgroup. They have traditionally been used for isolating membrane protein complexes due to their tendency to break lipid-lipid interactions rather than perturb protein–protein interactions [1]. Triton X-100, hereby referred to as TX-100, has a headgroup consisting of 9–10 EO units and is one of the most widely used surfactants for this purpose [2–6]. The lipid solubilization pathways of the detergent and the intermediate and final structures formed can be of critical importance to the structure and function of the membrane proteins being isolated – for example, in one case the markedly higher protein reconstitution in the presence of TX-100 [7] was attributed to the solubilization pathway of the surfactant. The solubilization mechanism of TX-100 has therefore been of particular interest and has been investigated extensively [6,8–19]. However, studies providing structural information on how TX-100 molecules interact with simple lipid bilayers are lacking, and many questions remain regarding the different stages of solubilization. In particular, how the detergent affects the bilayer in the partition stage and what structures are present at low concentrations has not been elucidated. Especially lipids in the gel phase display some irregularities in their behavior in the presence of TX-100.

Schnitzer *et al.* studied the solubilization of 1,2-dipalmitoyl-*sn-glycero*-3-phosphocholine (DPPC) bilayers at different temperatures over time by monitoring the absorbance of the solution and found that below the transition temperature, solubilization proceeded both *inefficiently*, requiring large amounts of detergent, as well as *slowly* [10]. They concluded that these effects were due to thermodynamic differences in the bilayer (such as bending and interstice energy) rather than kinetic factors [10]. In contrast, it was later found that non-sonicated, large unilamellar vesicles (LUVs) of DPPC in the gel phase were saturated and solubilized at a lower detergent concentration compared to DPPC above the phase transition temperature [9]. Most studies of the solubilization of phospholipid vesicles by TX-100 have also found an apparent growth of the vesicles at sub-solubilizing concentration of the detergent [20,21], attributing this either to the simple adsorption of TX-100 into the bilayers, thereby increasing the number of molecules in the vesicles [22], or to the fact that the detergent somehow facilitates fusion between the vesicles [20,21]. TX-100 has also been found to easily flip across lipid membranes affecting the efficiency of solubilization and making TX-100 a "fast" solubilizing detergent [23]. Possible intermediate structures with TX-100 as a fast solubilizer then include perforated vesicles, open-vesicular intermediates, and elongated worm-like micelles [21,23].

In this paper we have studied how TX-100 interacts with DPPC vesicles in the gel phase showing that, under certain conditions, a complex multilayered disc structure forms. We elucidate the structural evolution and morphological transition following the process both in space and time. For this purpose, we use a combination of scattering and imaging techniques. Small angle X-ray/neutron scattering (SAXS/SANS) measurements allow us to deduce nanoscale details on the structures present in solution without perturbing the samples, in particular the formation of multilayered bilayers with distinct, well-defined, periodic ripples. Cryo-transmission electron microscopy (cryo-TEM) and tomography (Cryo-ET) complement the scattering findings by providing a direct visualization of the nanodisc structures. These are formed upon addition of TX-100 to unilamellar DPPC vesicles and remain highly uniform over a rather broad range of different TX-100 concentrations. We speculate that structure may be induced by a combination of dehydration of the lipid headgroup by ethylene oxide headgroups of inserted TX-100 and remaining osmotic pressure of the free micelles/detergents. Detergents that are flipped to the inner leaflet may alter the water packing that, in combination with the osmotic pressure due to the mismatch in detergent concentration with the outside of the vesicles, might lead to a net attraction between bilayers. The rippled structure of the nanodiscs is hypothesized to occur due to the curvophilic nature of TX-100, causing it to segregate and make ordered line compressions. This segregation of TX-100 molecules causes a sawtooth like cross-section of the bilayer surface, where TX-100 accumulated in the positively curved peaks on each side of the leaflets. The arrangement allows most of the lipids to remain in a gel state due to the long wavelength of the ripples (26 nm) and stabilizes the structure from solubilization. This information sheds light upon the complexities involved in the interaction of surfactants with lipid membranes and why a wide range of seemingly different observations can be reported in the solubilization processes for lipid:surfactant systems that are perhaps assumed to be following the same pathways.

2. Materials and methods:

2.1. Preparation of samples

1,2-dipalmitoyl-*sn-glycero*-3-phosphocholine (DPPC, CAS: 63–89-8) and 1,2-dipalmitoyl-d62-*sn-glycero*-3-phosphocholine-1,1,2,2-d4-N,N,*N*-trimethyl-d9 (DPPC-d75, CAS: 181041–62-3) were purchased in powder form from Avanti Polar Lipids, Inc. Triton X-100 was purchased from Sigma-Aldrich.

Small unilamellar lipid vesicles (SUVs) of DPPC were prepared following standard procedures as recommended by Avanti Polar Lipids. DPPC powder was weighted into a round-bottom flask and dissolved in a 3:1 mixture of chloroform and methanol. A dry lipid film was then produced by evaporating the solvent under a flow of nitrogen gas and then leaving it under vacuum. An appropriate volume of 50 mM Tris buffer (pH 7.4) was added to the film to hydrate the lipids to form polydisperse multilamellar liposomes at a concentration of 5 or 10 mg/ml. To reduce multilamellarity, the DPPC solutions were sonicated for 20–30 min before extruded at 45 °C − 21 times through 100 nm filters and 21 times though a 50 nm filter. The sample was left at room temperature (∼20°) to cool down. Contrast matched vesicles were produced using the same protocol with the lipid powder being weighted out corresponding to 57.5 mol-% d-DPPC and 42.5 mol-% h-DPPC, and the buffer for hydrating the lipid film being made by a mixture 68% D_2O and 32% H_2O Tris buffer.

Stock solutions of 80 mg/ml TX-100 were prepared by dissolving the appropriate weight of detergent in the Tris buffer. For the SANS experiment, the same 68% D_2O and 32% H_2O Tris buffer as

used for the contrast matched lipids was used. Dilutions were made from the stock solution to give different concentrations of TX-100.

For the static SAXS and SANS measurements the detergent solutions were mixed into an equal volume of DPPC-vesicles and incubated for ∼ 10 h at 20 °C. In case of the SANS measurement and corresponding SAXS measurement of the contrast matched vesicle samples, the concentration of lipid was 5 mg/ml for all the measurements. For the SAXS measurements of the hydrogenated DPPC vesicles the concentration of lipid was 2.5 mg/ml. For the time-resolved SAXS measurement, stock solutions of 5 mg/ml DPPC and double the concentration of the wanted final TX-100 concentration was filled into the stopped-flow syringes for mixing by the stopped-flow apparatus.

2.2. Small angle X-ray and neutron scattering measurements

The static small angle X-ray scattering (SAXS) data was collected at the BioSAXS beamline BM29 [24,25] at the European Synchrotron Radiation Facility (ESRF) both before and after the synchrotron upgrade that finished in 2020. Both storage and exposure temperatures were set to respective temperature of the measurement as indicated in the results. 50 µL of each sample were loaded from the storage by the automated sample changer and measurements were performed at an energy of 0.995 Å with the samples in-flow to prevent radiation damage through a quartz glass capillary of 1 mm diameter. 10 frames of 0.5 s each were taken of each sample. The distance from the capillary to the Pilatus1 1 M (before upgrade) and Pilatus3 2 M (after upgrade) detector was 2.867 m. The buffer was measured before and after each sample measurement (with cleaning between). Data scaling and azimuthal integration to 1D-curves were performed on the 2D-detector images by the software at BM29. The data were set to absolute intensity scale with water as a primary standard. The SAXS curves for each individual frame in the sample and buffer was checked for radiation damage before averaging and subtraction of average buffer curves from average sample curves to give the final SAXS curves presented in this paper.

Small angle neutron scattering experiments were performed at the SANS-1 beamline at the Swiss Spallation Neutron Source SINQ [26]. The samples were mixed and filled into quartz cuvettes (110-QS of 1 mm and 2 mm thickness) at room temperature (∼20 °C) and then kept in the sample holder (at 20 °C) mounted in the sample table for the instrument. The samples were measured at 2 and 8 m detector distances with corresponding collimator distances of 4.5 m and 8 m with neutron beam of wavelength 0.7 nm. The BerSANS software [27] was used for data processing, including radial averaging, correction for electronic background and empty cell and normalization to absolute scale by using water measurements as a standard. The buffer measurements were subtracted from the sample measurements and the SAXS curves from the different distances were merged at overlapping Q-range.

Time-resolved SAXS and WAXS data were collected at the ID02 beamline [28] at the ESRF. The stopped-flow device was used for rapid mixing of the two components before transfer to the measurement capillary within 2.5 ms. The SAXS detector distance was 2 m and measurements were performed at a wavelength of 0.995 Å. The exposure time was 0.005 s for the initial kinetic run of 400 s (50 acquisitions) and then 0.05 s for measurements performed after (10 acquisitions per measurement). The measured SAXS and WAXS patterns were normalized and azimuthally averaged to obtain the one-dimensional profiles. Averaging of curves, background subtractions and binning of data was done in the SAXSutilities2 software. All fit analyses of SAXS data were performed using the QtiSAS software developed by Vitaliy Pipich [29].

2.3. Cryo-transmission electron microscopy and tomography

Transmission electron cryo-microscopy and cryo-tomography were performed at the Florence Center for Electron Nanoscopy (FloCEN, c/o Department of Chemistry "Ugo Schiff", University of Florence, Italy). Samples were prepared by applying ∼ 3 µL of DPPC or DPPC/TX-100 solutions onto freshly glow-discharged grids (Quantifoil R2.2 Cu Mesh 300, Germany) kept at 100% humidity and 20 °C. In order to allow the formation of a thin (ideally ≤ 200 nm) layer of amorphous ice with the samples embedded within, the grids were blotted with filter paper for 1 *sec*, blotting force 0, and then quickly plunge frozen in liquid ethane by using a dedicated device, such as the Vitrobot Mark IV (Thermo Fisher Scientific™). Micrographs were recorded on a Thermo Fisher Scientific™ Glacios™ microscope equipped with X-FEG high-brightness gun at 200 keV and a Falcon 3 camera (Thermo Fisher Scientific™) operated in linear mode. Nominal magnification was set at 36000x and 92000x for a calibrated pixel size of 4 Å and 2.5 Å, respectively. Total dose of ∼ 55 e⁻/Å² was spread over an exposure time of 2 *sec* with defocus value −5.0 µm. Micrographs were acquired via the EPU control software (Thermo Fisher Scientific™). Electron cryo-tomography tilt-series were acquired via the Tomography control software (Thermo Fisher Scientific™) spanned from −60° to + 60°, at 3° increment around a single axis. Each tilted image was exposed for 0.15 *sec* with a defocus value of −10.0 µm and received a dose of ∼ 2.9 e⁻/Å² – resulting in a cumulative dose of ∼ 114 e⁻/Å². Pixel size was set at 7.9 Å. Reconstruction of CTF corrected tilt-series was done via an iterative reconstruction scheme (SIRT) implemented in the IMOD software package [30] and the software Tomviz [31] was used to produce 3D rendering of the tomograms. In Tomviz the tomogram was first processed by applying a *gaussian filter* and a data transformation (*custom transform*) to remove noise and to obtain size manageable data, respectively. Successively, by using the *volume* operator a 3D rendering of the whole 3D stack was obtained, which was later cropped to the volume of interest. Finally, a *thresholding* filter was applied to the cropped volume to sharpen the contours of the objects [32,33].

2.4. Dynamic light scattering measurements

Dynamic light scattering measurements were performed at the Department of Chemistry, University of Oslo with the LS spectrometer by LS Instruments (Fribourg, Switzerland). The sample was mixed and transferred to glass tubes and inserted into the sample holder, while monitoring the time. The sample was then measured over time from mixing at 20 °C at a 90° scattering angle, with 30 s for each measurement.

3. Results and Discussion:

3.1. Characterization of rippled bilayer structures formed by TX-100 addition

Fig. 1 displays SAXS and SANS measurements of mixtures of vesicles consisting of 57.5% d-DPPC and 42.5% h-DPPC with different concentrations of TX-100 in 68% D₂O and 32% H₂O Tris buffer. (Measurements of these mixtures were also performed in pure H₂O Tris buffer shown in Fig. 5a, where we can see that the structural changes are unaffected by deuteration of the solvent). The SAXS pattern of the DPPC solution in absence of any TX-100 (1:0) in 1a) shows that the sample largely consists of unilamellar vesicles. There are no Bragg peaks in the bilayer scattering in the high Q-range (0.08–0.3 Å⁻¹) and there is an oscillation characteristic of the spherical form factor just above 0.01 Å⁻¹ allowing us to deduce
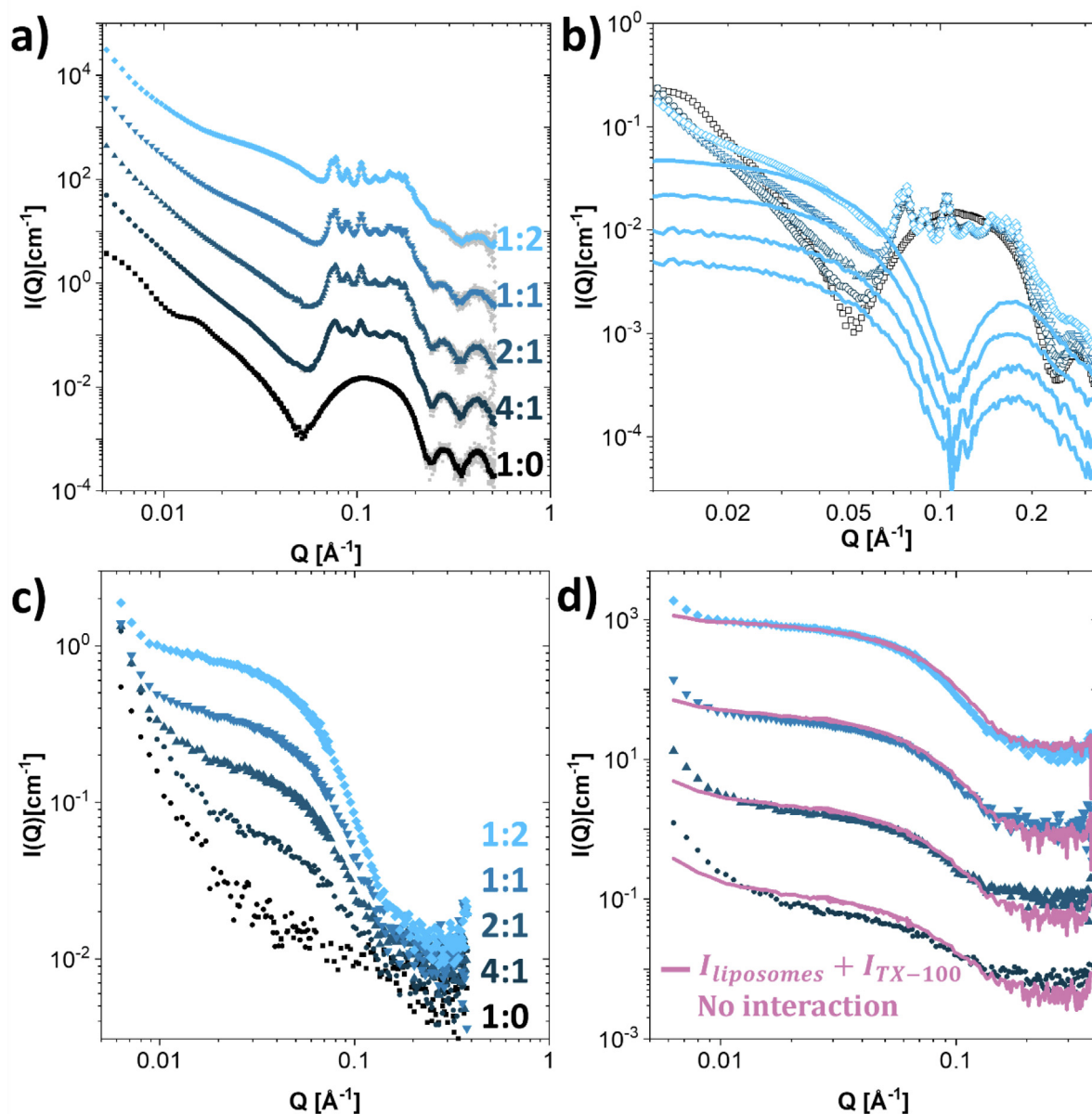
Fig. 1. **Detection of rippled structure upon TX-100 addition to DPPC bilayers.** Concentration of lipid was always 5 mg/ml, whereas the concentrations of TX-100 in mg/ml were 1.25, 2.5, 5.0, 10.0 for the 4:1, 2:1, 1:1 and 1:2 mixtures respectively. a) SAXS measurements (logarithmically scaled for visualization) of DPPC mixed with Triton X-100 in 68 % D_2O at mass ratios indicated on the right. b) SAXS measurements of pure TX-100 solutions at different concentrations (lines) laid on top of the unscaled measurements of the same DPPC:TX-100 mixtures as in a) to illustrate the large contribution from the free micelles. c) SANS measurement of near contrast matched DPPC (68% D_2O) mixed with Triton X-100 at mass ratios indicated on the right. d) SANS measurements from mixtures in c) compared with the sum of the intensity contributions of the pure DPPC and respective TX-100 measurement plotted as the pink line, which would be the expected intensity if there was no interaction between the components. (For interpretation of the references to colour in this figure legend, the reader is referred to the web version of this article.)

that average diameter of the vesicles is around the expected 50 nm. The smearing of this oscillation gives an indication of the polydispersity of the sample which we approximated to follow a Gaussian distribution. Using the found relative width, $\sigma = 0.35$, we can estimate the polydispersity index to be about $PDI = \sigma^2 + 1 = 1.12$. As TX-100 is added to the solution we see that Bragg peaks become visible on top of the characteristic broad maximum of the scattering originating from the bilayer. The peak pattern remains unchanged for different mass ratios of DPPC:TX-100 and are clearly different from Bragg peaks arising from the diffraction occurring due to the simple spacing between bilayers in a multilamellar vesicle; model simulations of multilamellar DPPC vesicles with different lamellar spacings d have been plotted in Figure S1 in the

supplementary information for reference. The peaks seem to be a superposition of several different repeat spacings that exist between different lamellar distances. Simultaneously, we see that the oscillation from the spherical form factor at around $Q = 0.01$ Å^{-1} has disappeared. As the concentration of TX-100 increases, the main change of the SAXS scattering is in the intermediate Q-range, consistent with an increase in TX-100 micellar units in solution as seen in Fig. 1b, where the corresponding pure TX-100 micelle measurements have been plotted along with those of the mixtures from Fig. 1a. Altogether, this makes it more difficult to elucidate the overall structure of the aggregates. Although we see that the bilayer structure is intact from the scattering at high Q, it is not possible to confidently say whether the aggregates are still

vesicular in nature. A similar pattern in the bilayer scattering has also been observed for the shorter chain lipid DMPC in our lab, although for lower temperatures and concentrations of TX-100 [34].

The used composition of h- and d-DPPC in the 68% D_2O and 32% H_2O solution allowed us to contrast-match the lipid vesicles in SANS, leaving mainly the TX-100 molecules visible in the total scattered intensity. The mixture of hydrogenated and deuterated lipid ensures that the headgroup has the same scattering length density as the tailgroup, and the mix of hydrogenated and deuterated water is then used to match this scattering length density (see Table S3 for overview). When adding TX-100 to the solution, only the scattering contribution from the TX-100 micelles and TX-100 inserted into the bilayer should be visible. As seen from Fig. 1c, the scattered intensity of the pure DPPC vesicles is very low, although some residual scattering is still present, thus the vesicle scattering was not completely matched to the solvent. However, since the intensity is much lower than that of TX-100, any large structural changes that could occur to the TX-100 structures would be visible. When TX-100 is added to the solution, a scattering pattern that resembles small spherical-like assemblies appears, which seems to be largely dominated by TX-100 micelles. The scattering from only TX-100 micelles (Figure S2) and only DPPC vesicle (seen in Fig. 1c as the 1:0 ratio) was also measured. The predicted scattering assuming no interaction between the two structures was calculated by a sum where the individual scattering contributions were weighted according to their concentrations in the mixture. This sum is drawn by the pink lines in the graph, and we see that there is a small change in the scattering pattern at the lowest Q value which must come from the larger lipid aggregates, as well as a slight decrease in the micellar scattering. These changes are most apparent in the mixture with the lowest TX-100 concentration. The SANS data therefore support the suggestion from the SAXS data that most of the TX-100 molecules still exist in their original micellar form, largely unchanged from the pure TX-100 micelles, and that only a very small number of TX-100 inserts into the larger lipid complexes. If these inserted TX-100 molecules do form any particular ordering in the bilayer, they are too few to give a sufficiently strong signal in the SANS measurement.

The patterns of peaks that occur at 20 °C in the pure DPPC lipid bilayers upon addition of TX-100 at concentrations above the CMC resemble those that have been collected for lipids in the well-known ripple phase [35,36]. The ripple phase occurs for lipid bilayers of saturated lipids between the gel phase and the fluid phase of the bilayer, and is characterized by a statistical sawtooth, rather than planar, structure of the bilayer [35,36]. Analysis of the observed reflections leads to the indices reported in Fig. 2a, that correspond to a monoclinic unit cell (*P*2), as illustrated in Fig. 2b. The values obtained for the repeat distance (d = 8.26 nm), oblique angle (107.3°) and wavelength (26 nm) are very close to those reported by Rappolt *et al.* for the metastable ripple phase of pure DPPC [37]. In that work, the metastable ripple phase was achieved by cooling the lipids from the liquid crystalline phase (compared to the stable phase which is achieved by heating) and is characterized by a more symmetric profile (rather than sawtooth-like). It was found to be stable for several hours although it can readily transform into the stable form over time [37,38]. The ripple phases are expected to occur right before the phase transition at ∼ 41 °C; from DSC data of the 50 nm DPPC vesicles, we see a peak at 35 °C which is likely the ripple phase in our case (Figure S3), far from the temperature of 20 °C where we have studied our samples. It is worth noting that we do not observe the ripple phase for unilamellar vesicles using SAXS since the multi-layers are required to get Bragg peaks, which suggests that the structures presented by the DPPC:TX-100 mixtures are quite consistently multi-layered.

To further investigate the structure that is present in the DPPC: TX-100 mixtures at 20 °C, cryo-TEM measurements were performed. Fig. 3a shows cryo-TEM images of DPPC lipid vesicles that were vitrified from 20 °C. The vesicles are not fully spherical as one might expect, but rather exhibit a faceted polygonal shape which is normally observed for small unilamellar vesicles in the gel phase [40]. We also see that we have a small fraction of bi-lamellar vesicles, which could also be deduced from model fits of the vesicles (Fig. 5a, 1:0 ratio). When we mix DPPC vesicle with TX-100 at a 1:1 ratio, larger structures with a highly ordered pattern of stripes can be observed. The different contrast of the stripes can arise from differences in thickness and/or electron density, i.e., brighter stripes would correspond to thinner regions and/or regions of average smaller electron density. Compared with the spherical vesicles, which show the maximal projection of the thickness at the edges of the shell compared to the center, lack of a defined edge on the striped structures suggests that they are more planar in nature than the pure lipid vesicles. We can only find the planar structures oriented parallel to the grid, suggesting that the bilayers must be rather rigid and do not bend much [41]. The structure seems to be independent of the concentration of TX-100 added – both higher and lower ratios have been measured with seemingly identical results; as an example a 2:1 DPPC:TX-100 mass ratio mixture
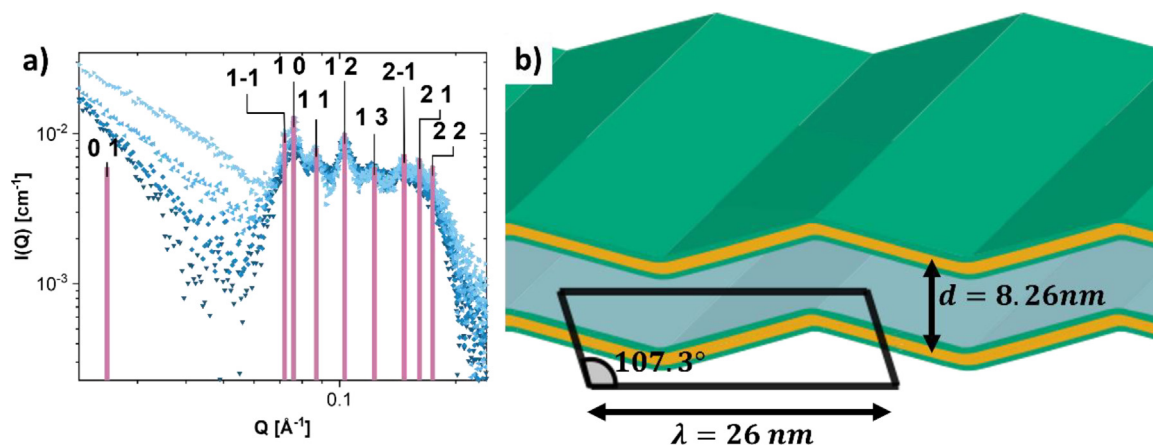

Fig. 2. Structure of bilayer ripples deduced from SAXS Bragg peaks. a) The reflections corresponding to the observed spacings of the ripple pattern found for the DPPC:TX-100 mixtures indexed on a monoclinic lattice of space group p2 are shown as pink bars. The obtained cell parameters are illustrated in b), using the definitions of Sun et al. [39]: the packing repeat distance, d, is equal to 8.26 nm, the ripple wavelength, λ, is 26 nm and the oblique angle is 107.3°. Note that the bilayer thickness is not representative of the real relative thickness but is drawn smaller for ease of visualization. (For interpretation of the references to colour in this figure legend, the reader is referred to the web version of this article.)
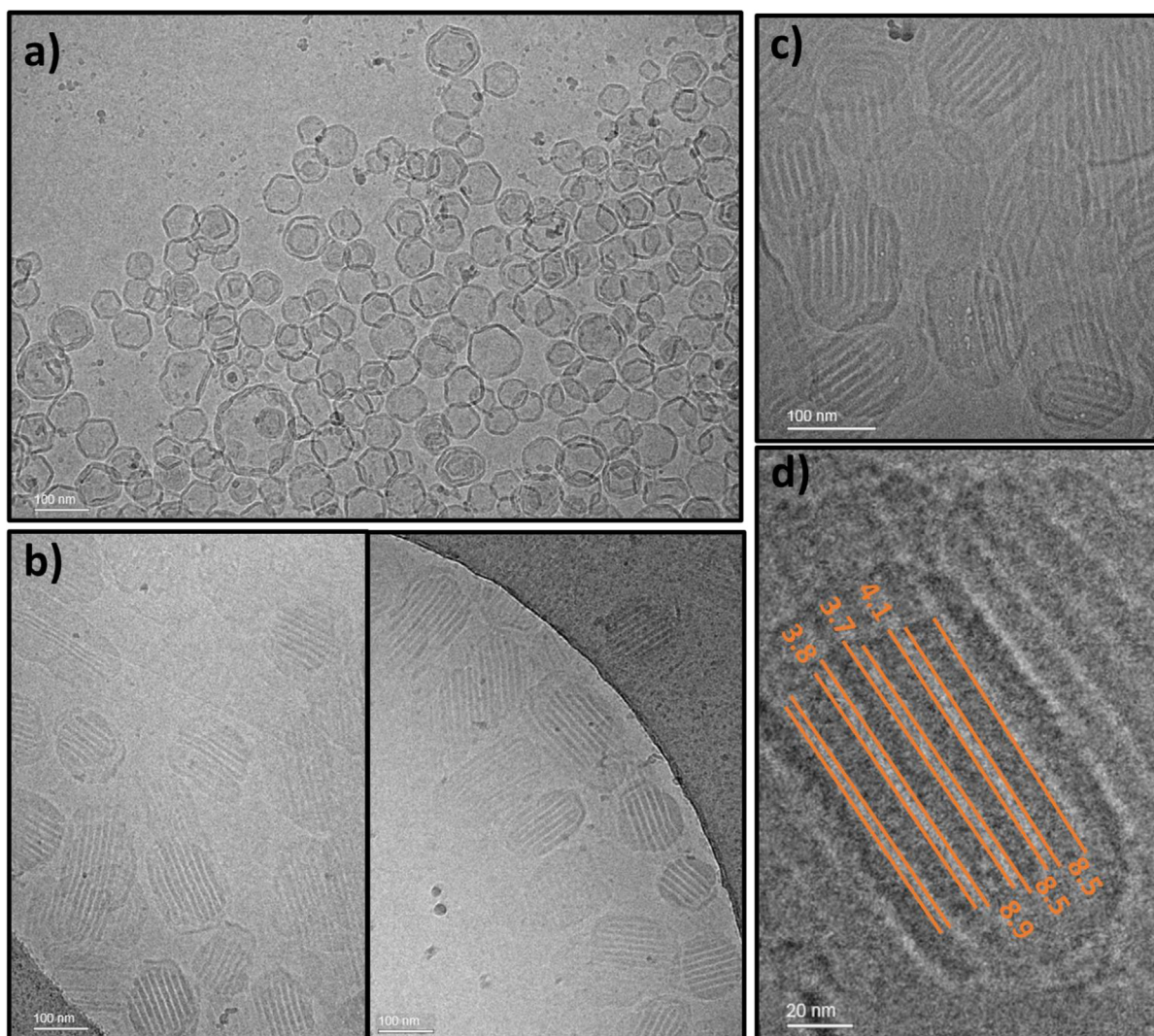
Fig. 3. Flat, striated bilayer structures observed in DPPC:TX-100 mixtures. Cryo-transmission electron microscopy images of a) DPPC liposomes, b) DPPC liposomes 5 mg/ml mixed with TX-100 5 mg/ml and incubated at 20 °C for 4 h, c) DPPC liposomes 5 mg/ml mixed with TX-100 1.25 mg/ml and incubated at 20 °C for 4 h, d) same mixture as in c, with measurements of stripe thicknesses.

is displayed in Fig. 3c. The pattern of stripes is also highly regular, with the higher density stripe being the thicker with about 8.5 nm in thickness and the lower density stripe the smaller with about half this thickness (Fig. 3d) giving a total repeat spacing of about 13 nm. Similar striated patterns in cryo-TEM images have been also connected with the ripple phase for DPPC bilayer [42,43]. No other significant structure can be found in these cryo-TEM images – all the lipid vesicles have been transformed into rippled nanodisc (additional images can be seen in Figure S4). From the SAXS and SANS data we assume that much of the TX-100 still exists as free micelles: due to the small defocus applied in order to prevent the nanodisc structures from damage, the micelles present too little contrast to be discerned in the images. The uniformity of structure in the solution is quite remarkable, since cryo-TEM studies of detergent:lipid mixtures at ratios that do not lead to complete solubilization of the vesicles into small micelles tend to reveal a wide variety of different structures in solution [44–50]. The spacing corresponds well with the wavelength found by the analysis of the reflections in the SAXS data assuming a model similar to that proposed by Vinson *et al.* previously where the spacing periodicity of the lines in the TEM images is expected to be half of the wavelength for the ripple phase [41].

Cryo-electron tomography was then performed on these samples to elucidate their three dimensional structure. Fig. 4 shows 3D renderings of representative striated bilayer structures, obtained from the measured tomograms using the software Tomviz (details in Methods and Materials section). The tomography image confirms that the striated structures are essentially planar, but not entirely flat, as they appear undulated, with the presence of several bending points. From the cross-section of the nanodisc structure we also confirm that it must be multilayered; this is most apparent in the videos showing rotations of some of the obtained tomograms provided in the supplementary information. A deduced thickness of about 11 nm fits well with an almost collapsed vesicle where two bilayers should be about 2 × 4.5 nm = 9 nm showing that most of the water in the vesicle interior is expelled. The dimensions fit well with the repeat distance deduced from SAXS (Fig. 2 b) of 8 nm, leading to a total dimension of about 12 nm. Additional animated 3D renderings are available in the SI.

To obtain further insight into the formation of the ripples it is interesting to compare the structure found for DPPC:TX-100 mixtures at 20 °C to the one found at even lower temperatures, where we do not observe the characteristic ripple pattern but do observe multilamellar structures [34]. Figure S5 displays cryo-TEM images
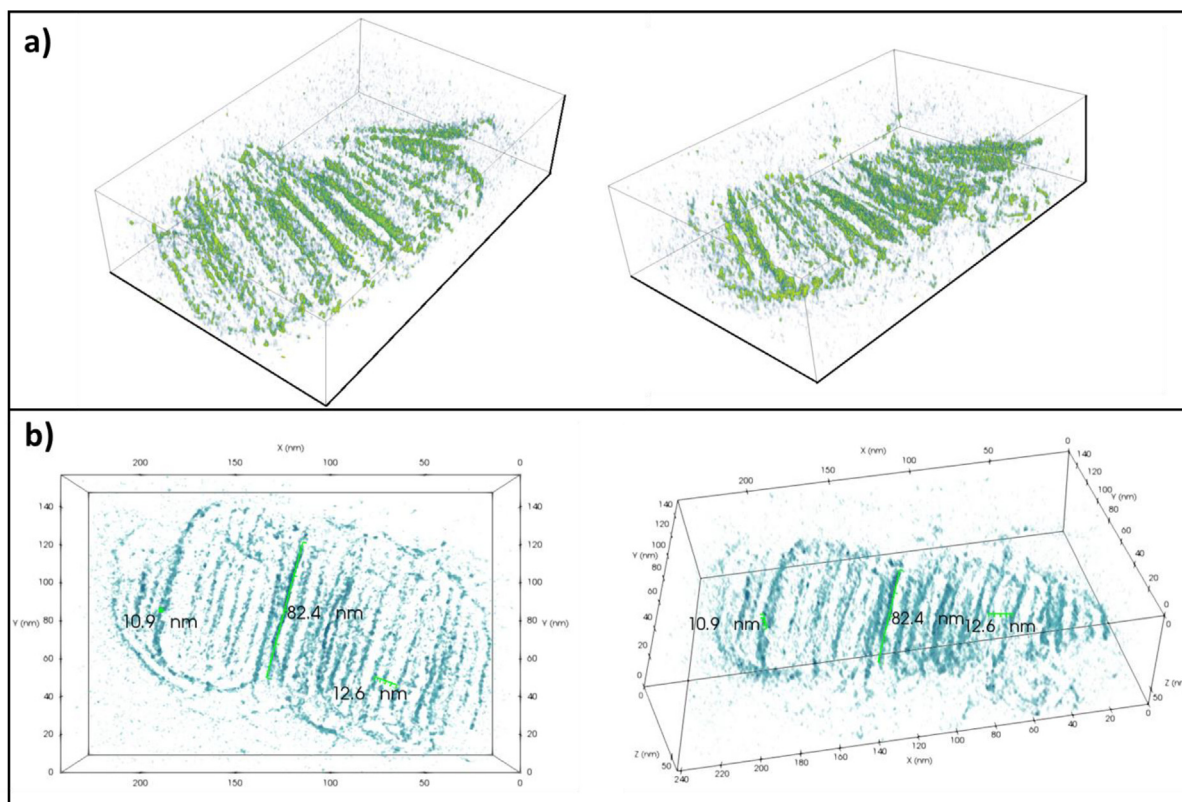
Fig. 4. Cryo-electron tomography images of structures formed in DPPC:TX-100 mixtures. a) 3D renderings of a representative structures revealed in the Cryo-transmission electron microscopy images of Fig. 2. Left and right figures represent the same structure visualized at different rotation angles. b) A representative structure with relevant length scales marked in figure. Thickness: 10.9 nm, width: 82.4 nm and distance between two stripes: 12.6 nm.

of samples that were vitrified from 10 °C. The pure DPPC vesicles diplay the same structures as at 20 °C, as expected. For the mixtures with TX-100, however, the vesicles seem to have transformed into stacks of lamellar sheets (Fig. S5b-c), causing the Bragg peaks in the SAXS pattern (Fig. S5d). The overall structure formed at 10 °C could therefore be the same as that formed at 20 °C, indicating that the formation of the striated structure is a thermodynamic transition state much like the ripple phase formation. We note that the results found here are characteristically different both in terms of the cryo-TEM and SAXS data from sheet-like structures that are formed when the bilayer fragments, which can be seen when TX-100 solubilizes the vesicles at higher temperature, as presented in a separate paper on solubilisation [34].

Since the structures formed are multilamellar in nature, it was of interest to also investigate how the introduction of a small amount of charge in the bilayer would affect the system. Fig. 5 compares the measurements for a pure DPPC system with added TX-100 to that of vesicles made up of 90 mol-% DPPC and 10 mol-% of the negatively charged lipid DPPG. The main transition temperature of DPPG is the same as for DPPC (∼41 °C)[51,52], thus we do not expect any large changes in the thermotropic phase of these vesicles compared to the pure DPPC vesicles. A measurement performed here at even lower TX-100 concentration (8:1) showed that for the pure DPPC system a simple multi-layered vesicle model can describe the data quite well (see SI section S6 for details, equation S17 correspond is the model used for the fits in Fig. 5a), affirming TX-100 can induce multilamellarity like observed in previous studies, but only displays the classical spherical multilamellar structures at low concentrations of detergent. It is worth noting that the concentration of TX-100 in this mixture is right around the CMC of TX-100 (∼0.3 mg/ml), and that the ripples themselves only

appear above this concentration. With the presence of a small amount of the charged lipid DPPG in the vesicles, no Bragg peaks are observed in the bilayer scattering upon TX-100 addition (Fig. 5b). From the fit analysis, it instead seems that the vesicles fragment into disc-like structures as more TX-100 is added, starting from the 2:1 ratio. The final discs at the higher TX-100 concentrations are polydisperse with an average radius of about 10 nm. The model used is that of a bicelle where Triton X-100 is allowed to distribute in surplus at the edges of the disc, forming a thick rim (see section S7 for details, equation S23 corresponds to the model used for the bicelle structures). Before formation of disc structures, we only see insertion of TX-100 into the bilayer (model described in S6, equation S17). These observations suggest that the introduction of charges causes the vesicles to undergo a completely different path upon addition of TX-100. With the charges preventing large deviations from a spherical structure in the vesicles, opening and disintegration of the vesicle is the more likely pathway taken. This provides open edges of the bilayer that are more available for further TX-100 insertion and eventual solubilization into large discs.

Differential scanning calorimetry measurements were also performed on the samples. Since, however, the complexes undergo irreversible solubilization when heated to the appropriate temperature, these results are rather difficult to interpret, and only the very first heat scan can possibly be representative for the structures studied in this paper. Figure S3 in the SI depicts nano-DSC measurements of the DPPC at different concentrations of TX-100. Only the sample with TX-100 at the lowest concentration (4:1 mass ratio) keeps the vesicle state during the heat scan; in this sample we can characterize new peaks in the temperature range from 23 to 29 °C, in addition to a shift in the main and pretransition
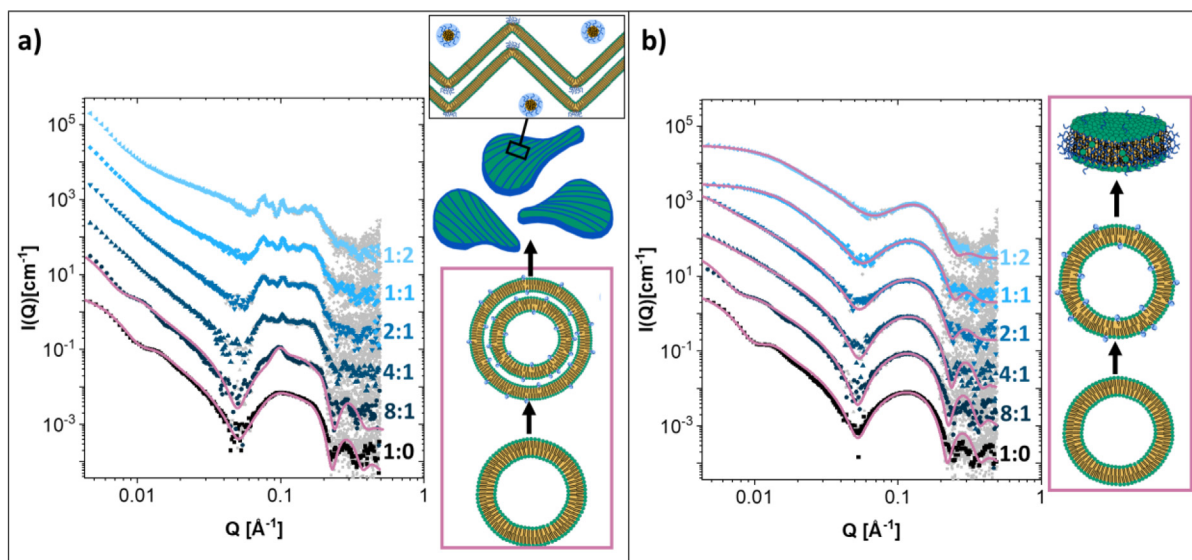
Fig. 5. Comparison of uncharged and charged vesicle response to TX-100. SAXS (logarithmically scaled for visualization) of vesicles a) of 100% DPPC lipids mixed with Triton X-100 at mass ratios indicated on the right and b) of 90% DPPC and 10% DPPG lipids mixed with Triton X-100 at mass ratios indicated on the right with model fits. These samples were incubated overnight (∼10 h) and measured at 20 °C. Models used for the model fits are illustrated to the right of the graphs inside the pink boxes. (For interpretation of the references to colour in this figure legend, the reader is referred to the web version of this article.)

temperatures. For the higher concentrations of TX-100 we mainly see peaks that are presumably related to the transition into mixed micelles.

3.2. Interpretation of results in terms of classical solubilization theory

Previous studies on DPPC and TX-100 mixtures suggest that DPPC is saturated and solubilized at lower concentrations in the gel phase as compared to the liquid crystalline phase [9]. The SAXS and SANS data revealed a large population of pure TX-100 micelles, indicating that the DPPC bilayers do become saturated at very low concentration when the temperature is far below the phase transition. Whether or not the product can be referred to as solubilized, however, is up for debate; while a size reduction might certainly occur when using very large vesicles, the lipid:TX-100 complexes that are formed are much larger than what would normally be considered a micelle and also possess "bilayer-like nature" even at high detergent:lipid ratios as seen from the cryo-TEM. Two key differences in our study are perhaps the use of small unilamellar vesicles compared to large ones and the use of a broader range of structural techniques. It is conceivable that TX-100 might have different effects on a larger, less curved bilayer, perhaps causing it to fragment into structures that are smaller relative to the LUVs while the resultant structures are more similar in size in the case of SUVs. The use of SAXS and cryo-TEM also gives structural information, whereas turbidimetry only allows for a qualitative detection of changes in size. Ahyayauch *et al.* also did NMR which showed that the lipids were in a much more rapidly tumbling environment, but only on sphingomyelin and TX-100 mixtures, not on PC-lipid mixtures [53]. Later NMR studies on detergent:lipid mixtures found a broadening of the Phosphorous-NMR signal with addition of TX-100 to egg-PC, attributed to formation of multilamellar vesicles, and the appearance of a sharp peak attributed to some lipid solubilization into micelles [54]. Such a broadening in the P-NMR signal could also be attributed to the structural changes reported for DPPC here.

Rather than referring to the solubilization process as occurring due to the "saturation" of the lipid membrane with detergent, some authors have deemed it more correct to separate between non-cooperative and cooperative binding to the membrane. Here it is proposed that the cooperative binding causes the bilayer to fragment due to detergent separation in the bilayer [55–57]. In fact, Kragh-Hansen *et al.* found that cooperative binding by dodecyl maltoside preceded the solubilization onset, forming holes in the membrane, and that rapid solubilization of the membrane required direct contact with the detergent micelles rather than solely free monomeric units [56]. Other authors have also observed pore formation in lipid bilayer by TX-100 [58]. We have not observed pore-like structures in any of the bilayer structures by cryo-TEM, but the rippled structures do seem to only appear above the CMC of TX-100, which could point to the possibility that cooperative binding is required for the formation of the striation in the bilayer.

Overall, the structural observations do not concur with the classical interpretation of how detergents interact and solubilize lipid membranes. The results illustrate how the small changes in the nature of the lipid system such as chain length, charges and temperature can lead to structures that are not associated with classical solubilization and that a complex combination of driving forces can make these complex structures surprisingly robust. Some of the quantitative changes, however, can be connected observations that have been considered as part of the initial stages of solubilization previously.

3.3. Kinetics of the transition from vesicles to flat, rippled structures

Time-resolved SAXS and WAXS measurements were performed on DPPC and TX-100 mixtures to investigate the kinetics of structure formation. Fig. 6 displays the resultant SAXS and WAXS patterns at certain timepoints after mixing the solutions. We see that after 55 ms the SAXS pattern overlaps almost completely with the calculated average of the scattering patterns for the individual solutions, suggesting that there is no change in the structure of neither lipid vesicles nor TX-100 micelles at this time-point. There is, however, a change in the WAXS-pattern where the peak has broadened, suggesting a change in the bilayer at the scale of the chain packing, possibly caused by the insertion of single TX-100 molecules. 2.3 s after mixing, there is also changes at very low Q, where the spherical oscillation becomes continuously more smeared out
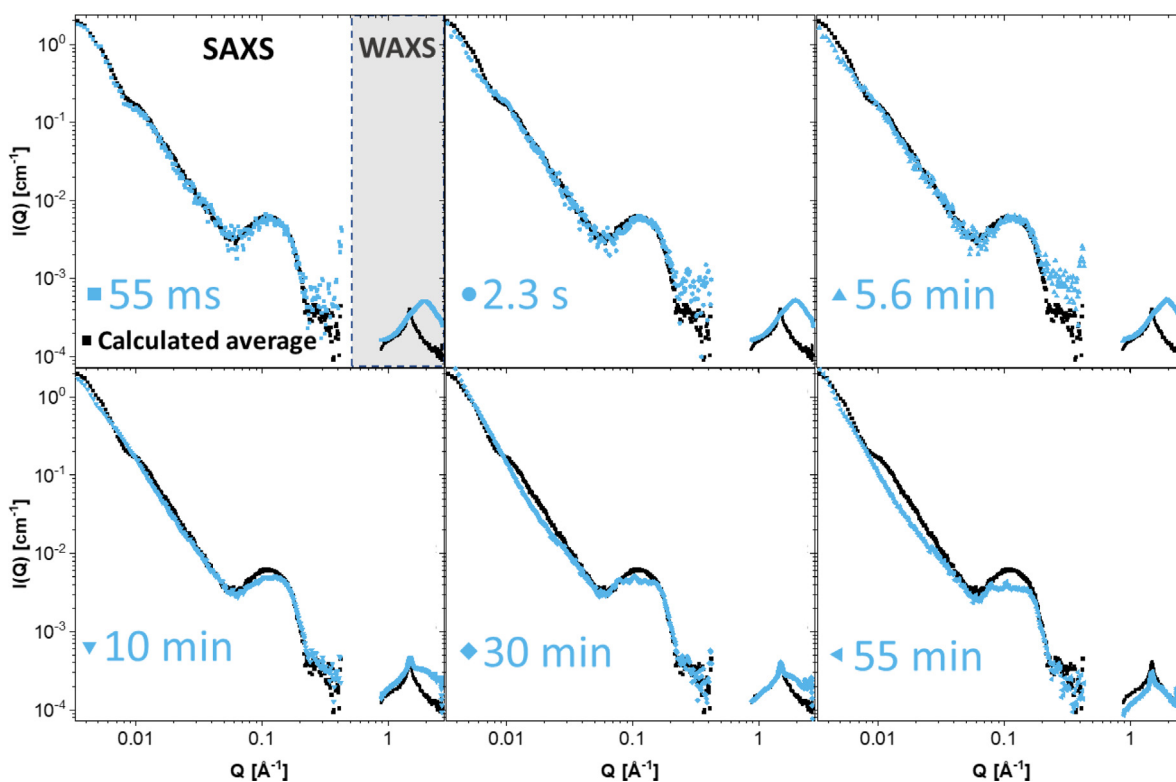
Fig. 6. Formation of structures seen in time. Time-resolved SAXS and WAXS measurements of a 1:1 mass ratio mixture of DPPC and TX-100. Calculated average shown in black for all different times is the sum of the individual DPPC and TX-100 scattering patterns.

and this change continues over the next minutes as seen also at the 5.6-minute timepoint. This could be attributed to an increase in size, but since there are no major shifts in the Q-position of the spherical oscillation it could also signify that the bilayers are collapsing or opening into the flatter structures, as seen by cryo-TEM and tomography. At 10 min the spherical form factor has completely disappeared, and changes start to occur in the bilayer scattering at intermediate Q values. This change is concurrent with the reappearance of the original DPPC peak in the WAXS pattern; although the bilayer structure is changing, the lipid chains seem to be returning to their original packing. At 30 min we can see the peaks starting to form in the bilayer scattering and the scattering at low Q continues to deviate further from the spherical vesicle scattering. These changes continue into the 55 min after mixing. At this point we see that although the overall structure, as indicated by the SAXS pattern, has drastically changed, the WAXS peak and therefore the lipid chain packing has returned to its starting point. Overall, the kinetics of the process show that the large structural changes going from vesicle to flattened structures seem to precede the local changes in the bilayer fluctuations. It is hypothesized that the structural changes in the bilayer, causing it to "ripple", allow the lipids to pack in a manner that is closer to their original gel state.

Dynamic light scattering measurements were performed for the 1:1 mixture, where the components (at 0.5 mg/ml) were mixed and then measured over time. It is likely that the timescale of the process is affected by the reduced concentration. Since the vesicles are no longer spherical after collapse, the hydrodynamic radius calculated from the Stokes-Einstein equation is only an apparent one. Nevertheless, it gives interesting, complementary information about the evolution of the overall nanostructure in time. Fig. 7a displays a selection of the obtained correlation functions which shows that the characteristic decay times increase with increasing elapsed time, demonstrating an increase in the

apparent hydrodynamic radius over time. CONTIN fit analysis of the size distribution displayed in Fig. 7b shows that not only the size decreases but also the relative polydispersity increases. The size increase is initially fast, but starts to equilibrate after about 1 h, as seen from Fig. 7c. The growth in the hydrodynamic diameter can be described remarkably well with a simple exponential growth with a characteristic time of about 38 min and provides an estimate of the limiting size of about 178 nm, cf. Fig. 7c. It is interesting to note that the overall intensity of SAXS at low Q and the overall intensity from light scattering was not found to vary over time. This suggests that the formation of the bilamellar nanodiscs is not caused by aggregation, fusion, or fission but rather an individual collapse of the vesicle itself. Given the rather slow time scale we speculate that the rate limiting steps are the organization of the surfactant and in particular the flipping of the surfactant to the inner leaflet causing instability and a net attraction between the opposing parts of the inner leaflet of the vesicles. To test this supposition, we can calculate the approximate diameter of flattened vesicles. The maximum size achieved by perfectly flattening the original vesicle[59] would be $\pi \times d/2 = 151 nm$, which fits rather well with a final dimension of 178 nm considering that additional swelling may be caused by the uptake of the surfactant and that the resultant flattened vesicles will not be perfectly circular.

3.4. What causes collapse of vesicles?

Many previous studies using light scattering have reported an increase in the hydrodynamic radius in mixtures with lower concentrations of TX-100 and for detergents in general [60]. Solubilization into smaller structures, however, comes from the theoretical consideration that detergents will generally favor higher curvature structures and thus would prefer insertion into smaller vesicles. Indeed, other surfactants that have been used to
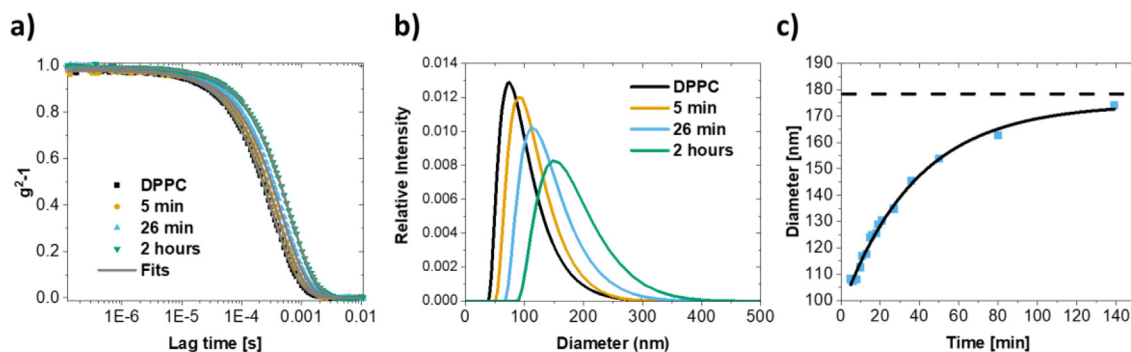
Fig. 7. Changes in hydrodynamic radius over time. a) Dynamic light scattering measurements of a 1:1 mass ratio mixture of DPPC and TX-100 (each component at 1 mg/ml). b) Size distributions at different timepoints from mixing resultant from a CONTIN analysis of the correlation function c) Time dependence of the hydrodynamic diameter found by cumulant analysis of the correlation function at different timepoints from mixing, with a fitted increasing exponential decay function starting at the diameter of the pure DPPC vesicles (96 nm) giving an upper bound of 178 nm and a rate constant of 0.026 min^{-1}.

produce spontaneously formed SUVs [48,61,62] cause transition from MLVs to SUVs [44]. In our results we do not observe any significant growth of the vesicle structure. Instead, the flat bilayer structures seen by cryo-TEM must either be vesicles that have opened and adhered or vesicles that have collapsed. Pore formations and opening of vesicular structures [63] have been observed previously, but the structures observed here seem to be multilamellar in all cases (see cryo-ET and the sharp peaks in the SAXS pattern). If the bilayers favor adhering to one another after TX-100 addition, it is likely that the vesicles would collapse when TX-100 flips into the inner leaflet. Since the dimensions of the structures observed by cryo-TEM are consistent with a flattening of the original vesicles, collapse of the vesicle structure seems the more likely scenario. A collapsed structure presents highly curved edges which could potentially accommodate surplus TX-100 molecules.

The flipping of TX-100 and thus the EO-headgroup to the inner leaflet of the vesicle could potentially play a role in the collapse of the vesicle structure. Membrane bound polyethylene glycol (PEG) surfactants have been preciously found to cause an increase of the repulsive force between bilayers [64]. In contrast, free PEG has been identified as a fusogenic agent [65–72], and similarly TX-100 has been suggested to lead to fusion of vesicles [17,21,45,57,73–75]. Sáez *et al.* also studied the effect of PEG preparations on lipid vesicles in an attempt to make a connection between TX-100 and PEG [76]: they saw that the behavior was similar, although it required much higher concentrations of PEG compared to TX-100 to achieve the same effect. Recently, it was also found by SANS and cryo-TEM also that when the nonionic surfactant-like polymer C$_{18}$-PEO4 interacted with DOPC vesicles, they transitioned from a unilamellar structure to a multilamellar structure [77]. All these results suggests that the addition of TX-100 should lead to bilayer attraction rather than repulsion. The physical mechanism of the attraction between the bilayers, however, is not entirely clear and needs further theoretical work. One suggestion for explaining apparent attraction and potential fusion of lipids in the presence of surfactants has been depletion forces that are caused by the exclusion of micelles from the bilayer surface [49,78]. Since our solutions have a very large amount of non-adsorbing TX-100 micelles, a depletion force could be thought to act between the inner leaflet due to the mismatch in concentration of the interior and exterior of the vesicles causing osmotic attraction [79]. This is further strengthened by the fact that the particles seem to collapse individually rather than forming multilamellar structures.

The origin of the repulsion between net electrically neutral, zwitterionic bilayers has been up for much debate [80,81] and the factors that cause a shift in the attractive-repulsive balance are thus not clear. The barrier for the adhesion of two bilayers involves the removal of some of the water between the two surfaces; however, the importance of water interactions versus surface interactions in opposing this dehydration is not clear. Studies of the interaction of C$_{12}$EO$_n$ with POPC membranes have shown that direct contacts between the lipid and detergent headgroup replaces water interactions causing a dehydration of the lipids and a reduction in the segmental mobility of the headgroups [82,83]. The data of König *et al.* are consistent with a scenario where the primary hydration shell remains intact for the lipids, whereas the more weakly bound water molecules are replaced by hydrated EO segments [83]. The repeat spacing of the lamellar POPC is also decreasing with the number of EO units of the surfactant [83,84]. This suggests that due to TX-100, the partial dehydration and change in conformational freedom of the lipids headgroups upsets the force balance that normally keeps the bilayers apart. An increase in the attractive force component through reduced freedom of orientation of the lipid headgroups and/or reduction of the repulsive component by removing or changing the polarization of the secondary water from the bilayer can be thought to redefine the optimal inter-distance of the bilayers. A plausible mechanism would then involve the inserted TX-100 molecules partially causing dehydration of the lipids and in addition being able to compensate for the highly curved edges of the formed nanodiscs. Interestingly, Burgess *et al.* also report a flattening of the vesicle structure upon addition of PEG, suggesting that the dehydration of the lipids plays an important role in the deformation of the vesicle structure without fusion [85]. Under the assumption that TX-100 incorporation into bilayers causes this type of bilayer attraction, why would our vesicles collapse rather than fuse and grow, like for example in the case of lecithin vesicles mixed with TX-100? Since our observations of the flat rippled structure is limited to DPPC vesicles at temperatures much under the transition temperature of the lipids, we can assume that the cause of this difference must partially lie in the phase of the lipids. Many of these same mixtures will be dissolved when mixed or heated to higher temperature, so the phase of the lipid clearly plays a very important role in the interaction [34]. Lecithin lipids are in a fluid phase, where TX-100 insertion is expected to cause less disturbance of the lipid packing as compared to the gel phase, thus allowing more TX-100 molecules to insert into the vesicles, potentially leading to a different shift in the attractive forces. When the bilayer contains a small amount of charge, the collapse of the vesicle structure is prevented by an additional repulsive force that is not present in the zwitterionic bilayers, thereby forcing a different pathway for the lipids to regain their favored pack-
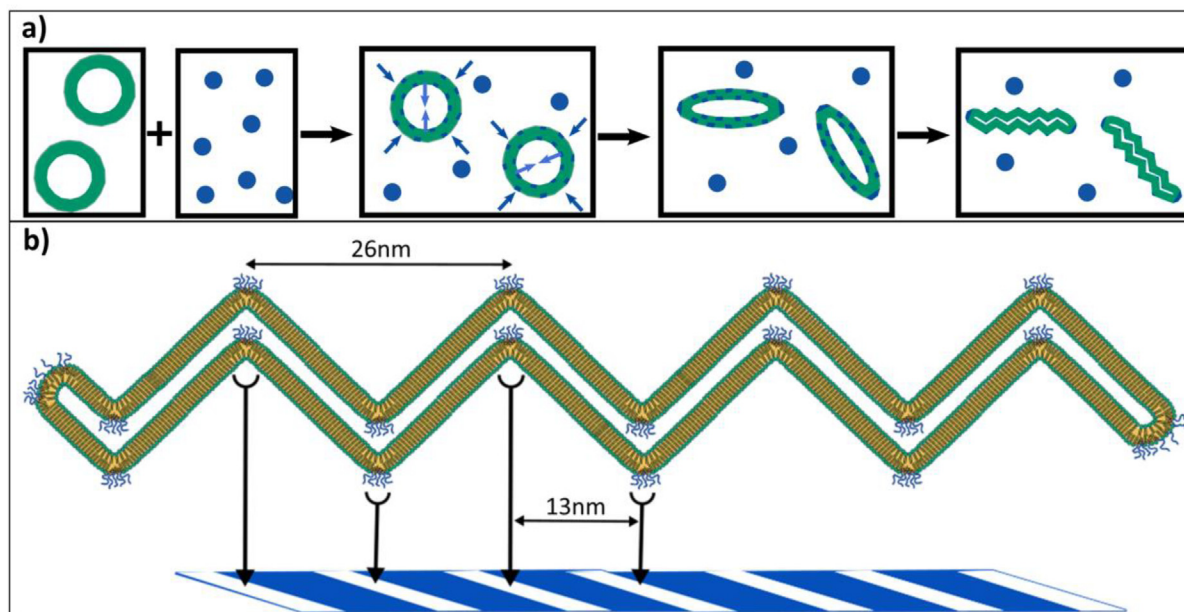
Fig. 8. The Formation of Rippled bilamellar Nanodisc. a) Illustration of possible steps in the formation of the rippled bilamellar nanodisc involving attraction between adjacent bilayers as TX-100 molecules insert into the vesicles leading to a collapse of the spherical lipid vesicles into a flat double bilayer followed by formation of ordered ripples. b) Illustration of a possible mechanism for TX-100 induced ripples in the bilayer and how it gives rise to the striped pattern in the cryo-TEM images.

ing. With aggregation and fusion also prevented by the repulsion from the charged lipids, the result is instead that the bilayers form open vesicular intermediates that then reduce in size as more TX-100 is accommodated, finally forming large disc-like structures. For the uncharged DPPC in the gel phase bilayers however, instead of solubilizing after collapse of the vesicles, the lipid bilayer rearranges into the rippled structure to accommodate the strain induced by inserted TX-100 on the packing in the bilayer.

3.5. The formation of a rippled bilayer: Possible mechanisms

The fact that TX-100 segregated to a larger extent into the rims of the discs formed upon interaction with the negatively charged lipid vesicles points towards the hypothesis that segregation of TX-100 molecules into defined domains also caused the rippled structure of the uncharged bilayers. Segregation of TX-100 in the lipid phase was observed by Fontaine *et al.*: in Langmuir monolayers of phospholipid on a detergent solution of TX-100, the adsorbed TX-100 segregated into pure lipid domains that were surrounded by detergent rich phases. This lead to compressions in the interphase between the two domains [86]. These studies also revealed that the monolayers remained resistant to solubilization if these areas of compression were allowed to exist; when the monolayers were expanded, solubilization of the phospholipids would occur. A similar process might be at work in our bilayer, although the ripples found in this study are more defined. More similar to our results, ordered line compressions were found in DPPC bilayers in interaction with TX-100 by Kirat *et al.* using atomic force microscopy on supported lipid membranes [87]. The tomography images also reveal that the stripes occur in the same line on the top bilayer as the adjacent bilayer in the stacked structure, showing that the ordering is not only laterally, but also adjacently in the bilayer. This is also the expected packing of the multilayers in the ripple structure according to the model of Vinson *et al.*[41]. We can then imagine the scenario illustrated in Fig. 8, where the TX-100 molecules segregate into the highly curved peaks of the ripples in the bilayer, both in the inner and outer leaflet. This is qualitatively consistent with the contrast observed in the cryo-TEM images: the TX-100

molecules induce thinning of the bilayer at the peaks of the ripples and by mixing with the lipids lower the average electron density of these regions. This preferential segregation could be seen as the driving force of the ripple formation since TX-100 would then be in a more micellar-like environment, whereas the lipids can remain in a packing state more like the gel phase, despite the bilayer no longer being planar. A gradual segregation of TX-100 into the high-curvature inflection points of the ripples would thus also explain the apparent reformation of the gel state inferred from the WAXS data in Fig. 6. Although the ripple wavelength is quite long, we must assume that this conformation does not require a very large number of TX-100 molecules since the SANS and SAXS data suggest that most of the detergent molecules remain in their pure micellar state.

Lastly, the rippled structure is not present at the lower temperature of 10 °C, even though the bilayer is still in the gel phase. It is possible that the bilayer at 10 °C allows less insertion compared to at 20 °C, but then we would still expect to see a rippled phase or at least the start of solubilization if we go high enough in concentration of TX-100. The force for segregation could also be even stronger at the lower temperature, causing TX-100 to segregation more highly for example in the edges of the flat structures.

Regardless, due to the similarity to the ripple phase of pure DPPC, the structure observed here should be seen as driven both by the detergent segregation but also by the accommodation of the preferred lipid packing in the membrane. The role of apparent attraction of bilayers due to the incorporation of TX-100 should also be recognized as a driving force for the uniformity of the structures.

4. Conclusions

In conclusion, we have monitored the morphological transition induced by addition of Triton X-100 to DPPC lipid vesicles using a range of structural techniques. Both cryo-TEM and SAXS data clearly show that below the melting point of the lipid gel phase, addition of TX-100 may lead to the formation of peculiar rippled bilamellar nanodiscs. A detailed analysis using contrast variation

SANS shows that very little TX-100 takes part in the formation of the ripples and most of the detergent molecules form free micelles. We speculate that this is a very important aspect leading to an imbalance in concentration with respect to the interior of the vesicles, hence leading to implosion and the formation of bilamellar nanodiscs. The collapse into nanodiscs is likely also induced by a shift in the attractive-repulsive balance of forces that exist between bilayer structures caused by the dehydration of lipid molecules by the inserted TX-100 molecules.

The mechanism for formation of the ripple structure is not entirely clear, but we speculate that the DPPC bilayers resist solubilization by the inserted TX-100 by rearrangement into a ripple phase where TX-100 is segregated into ordered line compressions. Since TX-100 can flip into the inner leaflet of the vesicle, this causes attraction and collapse of the vesicle structure into bilamellar sheetlike structures. Our observations have elucidated the structures formed in TX-100 and lipid vesicle mixtures at low temperature where the bilayer structure is resistant to solubilization into micellar aggregates and hypothesized on the changes in forces and bilayer structure that occurs to facilitate the formation of solubilization resistant bilayer bilamellar nanodiscs.

This study started with the question of how TX-100 interacted with and solubilized membranes at different temperatures. Instead of the expected insertion followed by solubilization into smaller units as predicted by the 3-stage model, we found that at low temperatures the DPPC vesicle membrane is not only highly resistant to solubilization, but that the large amount of TX-100 that remains in the pure micellar state combined with a small amount of insertion causes an apparent collapse of the vesicle structure. In addition, the rather small amount of inserted TX-100 can cause drastic changes in the lateral structure of the bilayer, where TX-100 is segregated into areas of high curvature so that most of the lipid molecules can keep their dense packing.

Although the solubilization of membranes by TX-100 has been extensively investigated in previous studies [8–10,12,13,16–21,88–93], most of these studies either used techniques which lack the structural resolution needed to observe the rippled nanodics, or the focus has been on higher temperatures where a solubilization of the lipid vesicles into smaller, more conventional micellar structures is observed, as we also report in a separate paper [34]. Our results support and help to further explain previous observations of Kirat *et al.* from atomic force microscopy on DPPC bilayers [87] as the SAXS data confirm the presence of a ripple phase, and the cryo-TEM additionally shows that the presence of TX-100 can induce a collapse of the vesicle structure. These findings highlight the rich phase behavior of rather simple mixtures of detergents and lipids that may have significant implication for the understanding of membrane systems relevant for biochemistry and biomedical applications. Moreover, our results also show that much remains to be fully understood with respect to the interactions and, in particular, the role of water in the structure and functioning of these systems. We thus foresee further studies of this system in the future using other techniques, both experimental and computational, that can further elucidate the forces that are at work in the system.

Data availability

Data will be made available on request.

Declaration of Competing Interest

The authors declare that they have no known competing financial interests or personal relationships that could have appeared to influence the work reported in this paper.

Author Information

Author Contributions

V.A.Bjørnestad: Conceptualization, Formal analysis, Investigation, Methodology, Software, Visualization, Writing - original draft. F. Soto-Bustamante: Investigation, Formal analysis, Visualization. G. Tria: Investigation, Formal analysis, Visualization. M. Laurati: Investigation, Methodology, Supervision, Writing - original draft. R. Lund: Conceptualization, Methodology, Supervision, Writing - review & editing.

Appendix A. Supplementary data

Supplementary data to this article can be found online at https://doi.org/10.1016/j.jcis.2023.03.037.

References

[1] A.M. Seddon, P. Curnow, P.J. Booth, Membrane proteins, lipids and detergents: not just a soap opera. *Biochimica et Biophysica Acta (BBA)* -, Biomembranes 1666 (1) (2004) 105–117, https://doi.org/10.1016/j.bbamem.2004.04.011.

[2] M.N. Jones, Surfactants in membrane solubilisation, Int. J. Pharm. 177 (2) (1999) 137–159, https://doi.org/10.1016/S0378-5173(98)00345-7.

[3] A. de la Maza, J.L. Parra, Solubilization of unilamellar phospholipid bilayers by nonionic surfactants, Colloid Polym. Sci. 272 (6) (1994) 721–730, https://doi.org/10.1007/BF00659286.

[4] M.A. Partearroyo, A. Alonso, F.M. Goñi, M. Tribout, S. Paredes, Solubilization of Phospholipid Bilayers by Surfactants Belonging to the Triton X Series: Effect of Polar Group Size, J. Colloid Interface Sci. 178 (1) (1996) 156–159, https://doi.org/10.1006/jcis.1996.0103.

[5] T. Nyholm, J.P. Slotte, Comparison of Triton X-100 Penetration into Phosphatidylcholine and Sphingomyelin Mono- and Bilayers, Langmuir 17 (16) (2001) 4724–4730, https://doi.org/10.1021/la001263+.

[6] D. Lichtenberg, H. Ahyayauch, A. Alonso, F.M. Goñi, Detergent solubilization of lipid bilayers: a balance of driving forces, Trends Biochem. Sci 38 (2) (2013) 85–93, https://doi.org/10.1016/j.tibs.2012.11.005.

[7] J. Knol, K. Sjollema, B. Poolman, Detergent-Mediated Reconstitution of Membrane Proteins, Biochemistry 37 (46) (1998) 16410–16415, https://doi.org/10.1021/bi981596u.

[8] A. Alonso, M.-A. Urbaneja, F.M. Goñi, F.G. Carmona, F.G. Cánovas, J.C. Gómez-Fernández, Kinetic studies on the interaction of phosphatidylcholine liposomes with Triton X-100. *Biochimica et Biophysica Acta (BBA)* -, Biomembranes 902 (2) (1987) 237–246, https://doi.org/10.1016/0005-2736(87)90301-4.

[9] H. Ahyayauch, M.I. Collado, A. Alonso, F.M. Goñi, Lipid bilayers in the gel phase become saturated by triton X-100 at lower surfactant concentrations than those in the fluid phase, Biophys. J. 102 (11) (2012) 2510–2516, https://doi.org/10.1016/j.bpj.2012.04.041 PubMed.

[10] E. Schnitzer, D. Lichtenberg, M.M. Kozlov, Temperature-dependence of the solubilization of dipalmitoylphosphatidylcholine (DPPC) by the non-ionic surfactant Triton X-100, kinetic and structural aspects, Chem. Phys. Lipids 126 (1) (2003) 55–76, https://doi.org/10.1016/S0009-3084(03)00093-8.

[11] P.A. Dalgarno, J. Juan-Colás, G.J. Hedley, L. Piñeiro, M. Novo, C. Perez-Gonzalez, I.D.W. Samuel, M.C. Leake, S. Johnson, W. Al-Soufi, et al., Unveiling the multi-step solubilization mechanism of sub-micron size vesicles by detergents, Sci. Rep. 9 (1) (2019) 12897, https://doi.org/10.1038/s41598-019-49210-0.

[12] O. López, A. de la Maza, L. Coderch, C. López-Iglesias, E. Wehrli, J.L. Parra, Direct formation of mixed micelles in the solubilization of phospholipid liposomes by Triton X-100, FEBS Lett. 426 (3) (1998) 314–318, https://doi.org/10.1016/S0014-5793(98)00363-9.

[13] S.K. Patra, A. Alonso, F.M. Goñi, Detergent solubilisation of phospholipid bilayers in the gel state: the role of polar and hydrophobic forces. *Biochimica et Biophysica Acta (BBA)* -, Biomembranes 1373 (1) (1998) 112–118, https://doi.org/10.1016/S0005-2736(98)00095-9.

[14] E. London, D.A. Brown, Insolubility of lipids in Triton X-100: physical origin and relationship to sphingolipid/cholesterol membrane domains (rafts). *Biochimica et Biophysica Acta (BBA)* -, Biomembranes 1508 (1) (2000) 182–195, https://doi.org/10.1016/S0304-4157(00)00007-1.

[15] B. Mattei, A.D.C. França, K.A. Riske, Solubilization of Binary Lipid Mixtures by the Detergent Triton X-100: The Role of Cholesterol, Langmuir 31 (1) (2015) 378–386, https://doi.org/10.1021/la504004r.

[16] Goñi, F. M.; Urbaneja, M.-A.; Arrondo, J. L. R.; Alonso, A.; Durrani, A. A.; Chapman, D. The interaction of phosphatidylcholine bilayers with Triton X-100. *European Journal of Biochemistry* **1986**, *160* (3), 659-665, https://doi.org/10.1111/j.1432-1033.1986.tb10088.x. DOI: https://doi.org/10.1111/j.1432-1033.1986.tb10088.x (acccessed 2022/04/09).

[17] Urbaneja, M.-A.; GoÑI, F. M.; Alonso, A. Structural changes induced by Triton X-100 on sonicated phosphatidylcholine liposomes. *European Journal of Biochemistry* **1988**, *173* (3), 585-588, https://doi.org/10.1111/j.1432-1033.1988.tb14039.x. DOI: (acccessed 2022/04/09).

[18] Partearroyo, M. A.; Urbaneja, M. A.; Goñi, F. M. Effective detergent/lipid ratios in the solubilization of phosphatidylcholine vesicles by Triton X-100. *FEBS Letters* **1992**, *302* (2), 138-140, https://doi.org/10.1016/0014-5793(92)80424-F. DOI: https://doi.org/10.1016/0014-5793(92)80424-F (acccessed 2022/04/09).

[19] C. Arnulphi, J. Sot, M. García-Pacios, J.-L.-R. Arrondo, A. Alonso, F.M. Goñi, Triton X-100 Partitioning into Sphingomyelin Bilayers at Subsolubilizing Detergent Concentrations: Effect of Lipid Phase and a Comparison with Dipalmitoylphosphatidylcholine, Biophys. J. 93 (10) (2007) 3504–3514, https://doi.org/10.1529/biophysj.107.104463.

[20] K. Nilsson, M. Almgren, W. Brown, M. Jansson, Effects of a Non-Ionic Surfactant on Small Unilamellar Lecithin Vesicles, Molecular Crystals and Liquid Crystals Incorporating Nonlinear Optics 152 (1) (1987) 181–203, https://doi.org/10.1080/00268948708070952.

[21] K. Edwards, M. Almgren, J. Bellare, W. Brown, Effects of Triton X-100 on sonicated lecithin vesicles, Langmuir 5 (2) (1989) 473–478, https://doi.org/10.1021/la00086a032.

[22] A. de la Maza, J.L. Parra, Assembly properties of Triton X-100/phosphatidylcholine aggregates during liposome solubilization, Colloid Polym. Sci. 274 (9) (1996) 866–874, https://doi.org/10.1007/BF00654745.

[23] D. Lichtenberg, H. Ahyayauch, F.M. Goñi, The mechanism of detergent solubilization of lipid bilayers, Biophys. J. 105 (2) (2013) 289–299, https://doi.org/10.1016/j.bpj.2013.06.007 PubMed.

[24] P. Pernot, A. Round, R. Barrett, A. De Maria Antolinos, A. Gobbo, E. Gordon, J. Huet, J. Kieffer, M. Lentini, M. Mattenet, et al., Upgraded ESRF BM29 beamline for SAXS on macromolecules in solution, J. Synchrotron Radiat. 20 (4) (2013) 660–664, https://doi.org/10.1107/S0909049513010431.

[25] A. Round, F. Felisaz, L. Fodinger, A. Gobbo, J. Huet, C. Villard, C.E. Blanchet, P. Pernot, S. McSweeney, M. Roessle, et al., BioSAXS Sample Changer: a robotic sample changer for rapid and reliable high-throughput X-ray solution scattering experiments, Acta Crystallogr. Sect. D 71 (1) (2015) 67–75, https://doi.org/10.1107/S1399004714026959.

[26] J. Kohlbrecher, W. Wagner, The new SANS instrument at the Swiss spallation source SINQ, J. Appl. Cryst. 33 (3 Part 1) (2000) 804–806, https://doi.org/10.1107/S0021889800099775.

[27] Keiderling, U. The new 'BerSANS-PC' software for reduction and treatment of small angle neutron scattering data. *Applied Physics A* **2002**, *74* (1), s1455-s1457. DOI: 10.1007/s003390201561.

[28] T. Narayanan, M. Sztucki, T. Zinn, J. Kieffer, J. Gorini, P. Van Vaerenbergh, P. Boesecke, Performance of the time-resolved ultra-small-angle X-ray scattering beamline with the Extremely Brilliant Source, J. Appl. Crystallogr. 55 (Pt 1) (2022) 98–111, https://doi.org/10.1107/s1600576721012693 From NLM.

[29] Pipich, V. *QtiSAS: user-friendly program for reduction, visualization, analysis and fit of SA(N)S data*" (2020). 2020. https://www.qtisas.com (accessed.

[30] J.R. Kremer, D.N. Mastronarde, J.R. McIntosh, Computer visualization of three-dimensional image data using IMOD, J Struct Biol 116 (1) (1996) 71–76, https://doi.org/10.1006/jsbi.1996.0013 From NLM.

[31] Hanwell, M. D. A., Utkarsh; Muller, David A.; Hovden, Robert;. *Tomviz project*tomviz.org (accessed 2022).

[32] B.D.A. Levin, E. Padgett, C.-C. Chen, M.C. Scott, R. Xu, W. Theis, Y. Jiang, Y. Yang, C. Ophus, H. Zhang, et al., Nanomaterial datasets to advance tomography in scanning transmission electron microscopy, Sci. Data 3 (1) (2016) 160041, https://doi.org/10.1038/sdata.2016.41.

[33] B.D.A. Levin, Y. Jiang, E. Padgett, S. Waldon, C. Quammen, C. Harris, U. Ayachit, M. Hanwell, P. Ercius, D.A. Muller, et al., Tutorial on the Visualization of Volumetric Data Using tomviz, Microscopy Today 26 (1) (2018) 12–17, https://doi.org/10.1017/S1551929517001213 From Cambridge University Press Cambridge Core.

[34] V.A.L. Bjørnestad, Pathways of membrane solubilization: a structural study of model lipid vesicles exposed to classical detergents, Langmuir (2023), https://doi.org/10.1021/acs.langmuir.2c03207.

[35] K. Akabori, J.F. Nagle. Structure of the DMPC lipid bilayer ripple phase. *Soft Matter* **2015**, *11* (5), 918-926, 10.1039/C4SM02335H. DOI: 10.1039/C4SM02335H.

[36] T.C. Lubensky, F.C. MacKintosh, Theory of "Ripple" Phases of Lipid Bilayers, Phys. Rev. Lett. 71 (10) (1993) 1565–1568, https://doi.org/10.1103/PhysRevLett.71.1565.

[37] M. Rappolt, G. Rapp, Structure of the stable and metastable ripple phase of dipalmitoylphosphatidylcholine, Eur. Biophys. J. 24 (6) (1996) 381–386, https://doi.org/10.1007/BF00576710.

[38] H. Yao, S. Matuoka, B. Tenchov, I. Hatta, Metastable ripple phase of fully hydrated dipalmitoylphosphatidylcholine as studied by small angle x-ray scattering, Biophys. J. 59 (1) (1991) 252–255, https://doi.org/10.1016/S0006-3495(91)82216-0 PubMed.

[39] W.J. Sun, S. Tristram-Nagle, R.M. Suter, J.F. Nagle, Structure of the ripple phase in lecithin bilayers, Proc. Natl. Acad. Sci. 93 (14) (1996) 7008–7012, https://doi.org/10.1073/pnas.93.14.7008 (acccessed 2022/09/05).

[40] A.E. Blaurock, R.C. Gamble, Small phosphatidylcholine vesicles appear to be faceted below the thermal phase transition, J. Membr. Biol. 50 (2) (1979) 187–204, https://doi.org/10.1007/BF01868948.

[41] P.K. Vinson, J.R. Bellare, H.T. Davis, W.G. Miller, L.E. Scriven, Direct imaging of surfactant micelles, vesicles, discs, and ripple phase structures by cryo-transmission electron microscopy, J. Colloid Interface Sci. 142 (1) (1991) 74–91, https://doi.org/10.1016/0021-9797(91)90034-6.

[42] A. Hicks, M. Dinda, M.A. Singer, The ripple phase of phosphatidylcholines: effect of chain length and cholesterol, Biochim. et Biophys. Acta (BBA) – Biomembr. 903 (1) (1987) 177–185, https://doi.org/10.1016/0005-2736(87)90167-2.

[43] E.J. Luna, H.M. McConnell, Lateral phase separations in binary mixtures of phospholipids having different charges and different crystalline structures, Biochim. et Biophys. Acta (BBA) – Biomembr. 470 (2) (1977) 303–316, https://doi.org/10.1016/0005-2736(77)90108-0.

[44] I.K. Mkam Tsengam, M. Omarova, E.G. Kelley, A. McCormick, G.D. Bothun, S.R. Raghavan, V.T. John, Transformation of Lipid Vesicles into Micelles by Adding Nonionic Surfactants: Elucidating the Structural Pathway and the Intermediate Structures, J. Phys. Chem. B 126 (11) (2022) 2208–2216, https://doi.org/10.1021/acs.jpcb.1c09685.

[45] A. Alonso, R. Sáez, A. Villena, F.M. Goñi, Increase in size of sonicated phospholipid vesicles in the presence of detergents, J. Membr. Biol. 67 (1) (1982) 55–62, https://doi.org/10.1007/BF01868647.

[46] Drescher, S.; Meister, A.; Garamus, V. M.; Hause, G.; Garvey, C. J.; Dobner, B.; Blume, A. Phenylene bolaamphiphiles: Influence of the substitution pattern on the aggregation behavior and the miscibility with classical phospholipids. *European Journal of Lipid Science and Technology* **2014**, *116* (9), 1205-1216,

https://doi.org/10.1002/ejlt.201300387. DOI: https://doi.org/10.1002/ejlt.201300387 (acccessed 2022/05/20).

[47] K. Edwards, M. Almgren, Solubilization of lecithin vesicles by C12E8: Structural transitions and temperature effects, J. Colloid Interface Sci. 147 (1) (1991) 1–21, https://doi.org/10.1016/0021-9797(91)90129-V.

[48] N.E. Gabriel, M.F. Roberts, Interaction of short-chain lecithin with long-chain phospholipids: characterization of vesicles that form spontaneously, Biochemistry 25 (10) (1986) 2812–2821, https://doi.org/10.1021/bi00358a012.

[49] M. Johnsson, K. Edwards, Interactions between Nonionic Surfactants and Sterically Stabilized Phophatidyl Choline Liposomes, Langmuir 16 (23) (2000) 8632–8642, https://doi.org/10.1021/la000190r.

[50] R. Sreij, C. Dargel, Y. Hannappel, J. Jestin, S. Prévost, R. Dattani, O. Wrede, T. Hellweg, Temperature dependent self-organization of DMPC membranes promoted by intermediate amounts of the saponin aescin, Biochim. et Biophys. Acta (BBA) – Biomembr. 1861 (5) (2019) 897–906, https://doi.org/10.1016/j.bbamem.2019.01.015.

[51] *Phase Transition Temperatures for Glycerophospholipids.* Avanti Polar Lipids, https://avantilipids.com/tech-support/liposome-preparation/lipids-for-liposome-formation (accessed 07/02/2023).

[52] J. Pan, F.A. Heberle, S. Tristram-Nagle, M. Szymanski, M. Koepfinger, J. Katsaras, N. Kučerka, Molecular structures of fluid phase phosphatidylglycerol bilayers as determined by small angle neutron and X-ray scattering, Biochim. Biophys. Acta 1818 (9) (2012) 2135–2148, https://doi.org/10.1016/j.bbamem.2012.05.007 From NLM.

[53] H. Ahyayauch, M.I. Collado, F.M. Goñi, D. Lichtenberg, Cholesterol reverts Triton X-100 preferential solubilization of sphingomyelin over phosphatidylcholine: A 31P-NMR study, FEBS Lett. 583 (17) (2009) 2859–2864, https://doi.org/10.1016/j.febslet.2009.07.046.

[54] M.G. Lete, B.G. Monasterio, M.I. Collado, M. Medina, J. Sot, A. Alonso, F.M. Goñi, Fast and slow biomembrane solubilizing detergents: Insights into their mechanism of action, Colloids Surf. B Biointerfaces 183 (2019), https://doi.org/10.1016/j.colsurfb.2019.110430 110430.

[55] M. le Maire, P. Champeil, J.V. Møller, Interaction of membrane proteins and lipids with solubilizing detergents, Biochim. et Biophys. Acta (BBA) – Biomembr. 1508 (1) (2000) 86–111, https://doi.org/10.1016/S0304-4157(00)00010-1.

[56] U. Kragh-Hansen, M. Le Maire, J.P. Noel, T. Gulik-Krzywicki, J.V. Moeller, Transitional steps in the solubilization of protein-containing membranes and liposomes by nonionic detergent, Biochemistry 32 (6) (1993) 1648–1656, https://doi.org/10.1021/bi00057a032.

[57] U. Kragh-Hansen, M. le Maire, J.V. Møller, The Mechanism of Detergent Solubilization of Liposomes and Protein-Containing Membranes, Biophys. J . 75 (6) (1998) 2932–2946, https://doi.org/10.1016/S0006-3495(98)77735-5.

[58] B. Mattei, R.B. Lira, K.R. Perez, K.A. Riske, Membrane permeabilization induced by Triton X-100: The role of membrane phase state and edge tension, Chem. Phys. Lipids 202 (2017) 28–37, https://doi.org/10.1016/j.chemphyslip.2016.11.009.

[59] U. Baxa, Imaging of Liposomes by Transmission Electron Microscopy, in: S.E. McNeil (Ed.), Characterization of Nanoparticles Intended for Drug Delivery, Springer, New York, 2018, pp. 73–88.

[60] D. Lichtenberg, E. Opatowski, M.M. Kozlov, Phase boundaries in mixtures of membrane-forming amphiphiles and micelle-forming amphiphiles, Biochim. et Biophys. Acta (BBA) – Biomembr. 1508 (1) (2000) 1–19, https://doi.org/10.1016/S0304-4157(00)00004-6.

[61] N.E. Gabriel, M.F. Roberts, Spontaneous formation of stable unilamellar vesicles, Biochemistry 23 (18) (1984) 4011–4015, https://doi.org/10.1021/bi00313a001.

[62] H. Hauser, N. Gains, H.J. Eibl, M. Mueller, E. Wehrli, Spontaneous vesiculation of aqueous lipid dispersions, Biochemistry 25 (8) (1986) 2126–2134, https://doi.org/10.1021/bi00356a042.

[63] A. Walter, P.K. Vinson, A. Kaplun, Y. Talmon, Intermediate structures in the cholate-phosphatidylcholine vesicle-micelle transition, Biophys. J. 60 (6) (1991) 1315–1325, https://doi.org/10.1016/S0006-3495(91)82169-5 PubMed.

[64] K. Arnold, O. Zschoernig, D. Barthel, W. Herold, Exclusion of poly(ethylene glycol) from liposome surfaces, Biochim. et Biophys. Acta (BBA) – Biomembr. 1022 (3) (1990) 303–310, https://doi.org/10.1016/0005-2736(90)90278-V.

[65] S.W. Burgess, D. Massenburg, J. Yates, B.R. Lentz, Polyethylene glycol-induced lipid mixing but not fusion between synthetic phosphatidylcholine large unilamellar vesicles, Biochemistry 30 (17) (1991) 4193–4200, https://doi.org/10.1021/bi00231a013.

[66] B.R. Lentz, Polymer-induced membrane fusion: potential mechanism and relation to cell fusion events, Chem. Phys. Lipids 73 (1) (1994) 91–106, https://doi.org/10.1016/0009-3084(94)90176-7.

[67] H. Wu, L. Zheng, B.R. Lentz, A slight asymmetry in the transbilayer distribution of lysophosphatidylcholine alters the surface properties and poly(ethylene glycol)-mediated fusion of dipalmitoylphosphatidylcholine large unilamellar vesicles, Biochemistry 35 (38) (1996) 12602–12611, https://doi.org/10.1021/bi960168q From NLM.

[68] J. Lee, B.R. Lentz, Evolution of Lipidic Structures during Model Membrane Fusion and the Relation of This Process to Cell Membrane Fusion, Biochemistry 36 (21) (1997) 6251–6259, https://doi.org/10.1021/bi970404c.

[69] J. Lee, B.R. Lentz, Outer Leaflet-Packing Defects Promote Poly(ethylene glycol)-Mediated Fusion of Large Unilamellar Vesicles, Biochemistry 36 (2) (1997) 421–431, https://doi.org/10.1021/bi9622332.

[70] B.R. Lentz, W. Talbot, J. Lee, L.-X. Zheng, Transbilayer Lipid Redistribution Accompanies Poly(ethylene glycol) Treatment of Model Membranes but Is Not Induced by Fusion, Biochemistry 36 (8) (1997) 2076–2083, https://doi.org/10.1021/bi9623340.

[71] A.R. Viguera, M. Mencia, F.M. Goni, Time-resolved and equilibrium measurements of the effects of poly(ethylene glycol) on small unilamellar phospholipid vesicles, Biochemistry 32 (14) (1993) 3708–3713, https://doi.org/10.1021/bi00065a024.

[72] A.-R. Viguera, A. Alonso, F.M. Goñi, Liposome aggregation induced by poly (ethylene glycol). Rapid kinetic studies, Colloids Surf. B Biointerfaces 3 (5) (1995) 263–270, https://doi.org/10.1016/0927-7765(94)01138-U.

[73] M.C.A. Stuart, E.J. Boekema, Two distinct mechanisms of vesicle-to-micelle and micelle-to-vesicle transition are mediated by the packing parameter of phospholipid–detergent systems, Biochim. et Biophys. Acta (BBA) – Biomembr. 1768 (11) (2007) 2681–2689, https://doi.org/10.1016/j.bbamem.2007.06.024.

[74] M.A. Urbaneja, J.L. Nieva, F.M. Goñi, A. Alonso, The influence of membrane composition on the solubilizing effects of Triton X-100, Biochim. et Biophys. Acta (BBA) – Biomembr. 904 (2) (1987) 337–345, https://doi.org/10.1016/0005-2736(87)90383-X.

[75] D. Velluto, C. Gasbarri, G. Angelini, A. Fontana, Use of Simple Kinetic and Reaction-Order Measurements for the Evaluation of the Mechanism of Surfactant-Liposome Interactions, J. Phys. Chem. B 115 (25) (2011) 8130–8137, https://doi.org/10.1021/jp2026187.

[76] R. Sáez, A. Alonso, A. Villena, F.M. Goñi, Detergent-like properties of polyethyleneglycols in relation to model membranes, FEBS Lett. 137 (2) (1982) 323–326, https://doi.org/10.1016/0014-5793(82)80376-1.

[77] J.U. De Mel, S. Gupta, L. Willner, J. Allgaier, L.R. Stingaciu, M. Bleuel, G.J. Schneider, Manipulating Phospholipid Vesicles at the Nanoscale: A Transformation from Unilamellar to Multilamellar by an n-Alkyl-poly (ethylene oxide), Langmuir 37 (7) (2021) 2362–2375, https://doi.org/10.1021/acs.langmuir.0c03302.

[78] M. Almgren, Mixed micelles and other structures in the solubilization of bilayer lipid membranes by surfactants, Biochim. et Biophys. Acta (BBA) – Biomembr. 1508 (1) (2000) 146–163, https://doi.org/10.1016/S0005-2736(00)00309-6.

[79] J.N. Israelachvili. *Intermolecular and surface forces*, 3rd ed.; Academic Press, 2011.

[80] E. Schneck, F. Sedlmeier, R.R. Netz. Hydration repulsion between biomembranes results from an interplay of dehydration and depolarization. *Proceedings of the National Academy of Sciences* **2012**, *109* (36), 14405-14409. DOI: 10.1073/pnas.1205811109 (acccessed 2022/08/18).

[81] B. Kowalik, A. Schlaich, M. Kanduč, E. Schneck, R.R. Netz, Hydration Repulsion Difference between Ordered and Disordered Membranes Due to Cancellation of Membrane-Membrane and Water-Mediated Interactions, J. Phys. Chem. Lett. 8 (13) (2017) 2869–2874, https://doi.org/10.1021/acs.jpclett.7b00977.

[82] F. Volke, A. Pampel, Membrane hydration and structure on a subnanometer scale as seen by high resolution solid state nuclear magnetic resonance: POPC and POPC/C12EO4 model membranes, Biophys. J. 68 (5) (1995) 1960–1965, https://doi.org/10.1016/S0006-3495(95)80373-5.

[83] B. König, U. Dietrich, G. Klose, Hydration and Structural Properties of Mixed Lipid/Surfactant Model Membranes, Langmuir 13 (3) (1997) 525–532, https://doi.org/10.1021/la960571y.

[84] G. Klose, A. Islamov, B. König, V. Cherezov, Structure of Mixed Multilayers of Palmitoyloleoylphosphatidylcholine and Oligo(oxyethylene glycol) Monododecyl Ether Determined by X-ray and Neutron Diffraction, Langmuir 12 (2) (1996) 409–415, https://doi.org/10.1021/la950383s.

[85] S.W. Burgess, T.J. McIntosh, B.R. Lentz, Modulation of poly(ethylene glycol)-induced fusion by membrane hydration: importance of interbilayer separation, Biochemistry 31 (10) (1992) 2653–2661, https://doi.org/10.1021/bi00125a004.

[86] P. Fontaine, M.C. Fauré, F. Muller, M. Poujade, J.-S. Micha, F. Rieutord, M. Goldmann, Unexpected Stability of Phospholipid Langmuir Monolayers Deposited on Triton X-100 Aqueous Solutions, Langmuir 23 (26) (2007) 12959–12965, https://doi.org/10.1021/la701293n.

[87] K.E. Kirat, A. Pardo-Jacques, S. Morandat, Interaction of non-ionic detergents with biomembranes at the nanoscale observed by atomic force microscopy, Int. J. Nanotechnol. 5 (2008) 769–783.

[88] H. Ahyayauch, C. Arnulphi, J. Sot, A. Alonso, F.M. Goñi, The onset of Triton X-100 solubilization of sphingomyelin/ceramide bilayers: effects of temperature and composition, Chem. Phys. Lipids 167–168 (2013) 57–61, https://doi.org/10.1016/j.chemphyslip.2013.02.003.

[89] H. Ahyayauch, M. Bennouna, A. Alonso, F.M. Goñi, Detergent Effects on Membranes at Subsolubilizing Concentrations: Transmembrane Lipid Motion, Bilayer Permeabilization, and Vesicle Lysis/Reassembly Are Independent Phenomena, Langmuir 26 (10) (2010) 7307–7313, https://doi.org/10.1021/la904194a.

[90] H. Ahyayauch, B. Larijani, A. Alonso, F.M. Goñi, Detergent solubilization of phosphatidylcholine bilayers in the fluid state: Influence of the acyl chain structure, Biochim. et Biophys. Acta (BBA) – Biomembr. 1758 (2) (2006) 190–196, https://doi.org/10.1016/j.bbamem.2006.01.016.

[91] A. Alonso, A. Villena, F.M. Goñi. Lysis and reassembly of sonicated lecithin vesicles in the presence of triton X-100. *FEBS Letters* **1981**, *123* (2), 200-204, https://doi.org/10.1016/0014-5793(81)80287-6. DOI: https://doi.org/10.1016/0014-5793(81)80287-6 (acccessed 2022/05/12).

[92] O. López, M. Cócera, R. Pons, N. Azemar, C. López-Iglesias, E. Wehrli, J.L. Parra, A. de la Maza, Use of a Dynamic Light Scattering Technique To Study the Kinetics of Liposome Solubilization By Triton X-100, Langmuir 15 (13) (1999) 4678–4681, https://doi.org/10.1021/la981473a.

[93] G. Ruderman, J.R. Grigera, Effect of Triton X-100 on the physical properties of liposomes, Biochim. et Biophys. Acta (BBA) – Biomembr. 863 (2) (1986) 277–281, https://doi.org/10.1016/0005-2736(86)90267-1.